Electronic supplementary information (ESI) for

Anisotropic thermal motion in transition-metal carbonyls from experiments and *ab initio* theory

Volker L. Deringer, Ai Wang, Janine George, Richard Dronskowski and Ulli Englert

Data collection and refinement

A suitable single crystal of **1** with approximate dimensions 0.20×0.18×0.13 mm^3 was glued to a glass fibre with two-component epoxy resin adhesive and then mounted on a goniometer head. The crystal was cooled from ambient temperature to 100 K over a period of 1 h, using an Oxford Cryosystems 700 open-flow cryostat. Details of the data collection are given in *Table S1*. All intensity data were collected on a Bruker D8 goniometer equipped with an APEX CCD area detector and an Incoatec microsource using Mo K radiation (λ = 0.71073 Å). Intensity data were integrated using the program SAINT+ [S1] and corrected for absorption by multi-scan methods with SADABS [S2].

Table S1 Crystal data and refinement results of **1** at full ($2\theta_{max}$= 109.83°) and limited resolution ($2\theta_{max}$= 89.98°).

Compound	$Cr(CO)_6$	
M_r	220.06	
Crystal system	orthorhombic	
Space group	*Pnma*	
a (Å)	11.5165(3)	
b (Å)	10.9267(2)	
c (Å)	6.21560(10)	
V ($Å^3$)	782.15(3)	
Z	4	
Crystal size (mm^3)	0.20×0.18×0.13	
no of parameters	67	
2*θ* (°)	109.83	89.98
Total / unique reflections	47979 / 5016	35569 / 3287
R_{int}	0.0640	0.0591
$(\sin\theta/\lambda)_{max}$ ($Å^{-1}$)	1.15	0.995
$R[F^2>2\sigma(F^2)]$	0.0360	0.0283
$wR_2(F^2)$	0.1054	0.0788
GOF	1.055	1.068
$\Delta\rho_{max}$ / $\Delta\rho_{min}$ (e $Å^{-3}$)	0.723 / –1.613	0.711 / –1.014

Data completeness and quality

Listing S1 Detailed information concerning data completeness and quality of **1** at full resolution (θ_{max}= 54.91°).

θ	sin θ/λ	Complete	Expected	Measured	Missing
20.82	0.500	0.998	438	437	1
23.01	0.550	0.998	577	576	1
25.24	0.600	0.999	748	747	1
27.51	0.650	0.999	943	942	1
29.84	0.700	0.999	1181	1180	1
32.21	0.750	0.997	1449	1445	4
34.65	0.800	0.998	1744	1740	4
37.17	0.850	0.995	2094	2083	11
39.77	0.900	0.991	2483	2461	22
42.47	0.950	0.992	2906	2883	23
45.29	1.000	0.986	3389	3343	46
48.27	1.050	0.987	3913	3862	51
51.43	1.100	0.980	4496	4408	88
54.82	1.150	0.979	5109	5004	105
54.91	1.151	0.979	5126	5016	110

Ab initio computation of ADPs

The computational procedure employed here consists of two steps. First, a full optimisation of the lattice and atomic positions is carried out, by minimising the total energy according to Hellmann–Feynman forces using standard procedures. The structure thus obtained hence refers to the true DFT-D minimum at 0 K, and is kept fixed during the following ADP computation. Previous work [S3], where we compared computed ADPs to temperature-dependent XRD data, indeed confirmed that this is a perfectly justified approach in the low-temperature regime up to 100 K [S4].

The prediction of ADPs itself is based on phonon computations which we perform using the finite-displacement method as implemented in PHONOPY [S5]. These computations are performed by slightly displacing all symmetry-inequivalent atoms in supercells constructed from the optimised crystal structures, and translating the forces on atoms so arising into force constants and then into the so-called *dynamical matrix*. From there, for each phonon mode *p* and reciprocal-space point *q*, PHONOPY determines the vibrational eigenvectors $\vec{e}_p^{\alpha}(q)$ and the frequencies or eigenvalues $\omega_p(q)$.

Once both the eigenvectors (where do the atoms move?) and eigenvalues (how strongly is a phonon mode active at a given temperature?) are known, they can be translated into atomic displacements. The mean-square displacement in a given Cartesian direction α is [S6]

$$\langle|\vec{u}^{\alpha}|\rangle^2 = \frac{1}{MN}\sum_{p,q}\left[\vec{e}_p^{\alpha}(q)\cdot\vec{e}_p^{\alpha}(-q)\frac{\hbar}{2\omega_p(q)}\left(1+\frac{2}{\exp\left(\frac{\hbar\omega_p(q)}{k_\mathrm{B}T}\right)-1}\right)\right]$$

and further expressions have been derived and implemented to yield the full anisotropic displacement matrix (see Ref. [S6] and the PHONOPY documentation). These are accessible in PHONOPY by setting the command `TDISPMAT = .TRUE.`; subsequently, the program's output can be conveniently converted to CIF format using a set of scripts we provide free of charge at www.ellipsoids.de.

We emphasise that careful convergence with regard to *q*-points is vital for a successful ADP computation [S3]. In the present case, we used *q*-point meshes of 64×64×128 for **1**, 90×50×90 for **2**, and 92×46×46 for **3**.

Regarding convergence parameters, we also tested the influence of the cutoff energy for the plane-wave expansion during the phonon computations; due to the large computational requirements, we performed this test for urea. We did this at the PBE+D3 level of theory. We used a *q*-point mesh of 50×50×55 and a frequency-cutoff of 0.15 THz for both calculations. In *Table S2*, we compare the ADPs computed with a plane-wave cutoff energy of 500 eV and of 700 eV. Clearly, the ADPs are converged with respect to this parameter at a cutoff of 500 eV (to within less than 1%).

Table S2 Comparison of computed equivalent displacement parameters for crystalline urea, illustrating the convergence of ADP computations with regard to plane-wave cutoff energy.

	U_{eq} (10^{-4} Å)	
Cutoff	**500 eV**	**700 eV**
C1	43.2	43.2
O1	58.6	59.1
N1	91.4	91.0
H1	220	219
H2	227	227

Comparison to high-resolution based multipole refinement for **2**

As discussed in the main text, a recent high-resolution charge-density study has been reported for **2**, where a multipole refinement allowed for a precise determination of the chromium, carbon, and oxygen ADPs in the crystal structure [S7]. As a further test of the validity of the *ab initio* method, we here compare predicted displacement parameters at 100 K to the above-mentioned, recent experimental result.

The results (*Table S3* and *Figure S1*) lend further support to the conclusions of the main text: the computational predictions are very close to the experimental ones, both regarding the magnitude and the anisotropy of the thermal motion.

Table S3 Comparison of equivalent displacement parameters for 2 at 100 K, obtained from multipole refinement ("Expt.", Ref. [S7]) as discussed in the main text, and from computations at the same level as applied throughout this work.

	U_{eq} (10^{-4} Å)	
	Expt.[S7]	**Computed**
Cr(1)	88	103
O(4)	277	280
O(5)	214	223
C(1)	130	144
C(2)	147	161
C(3)	163	176
C(4)	156	166
C(5)	133	143
H(1)	*255*[a]	*325*
H(2)	*360*[a]	*359*
H(3)	*285*[a]	*386*

[a]As discussed in Ref. [S7], the hydrogen ADPs were not obtained from refinement but by scaling the previously reported neutron-derived values (as cited in the main manuscript). They are hence not part of the following visual comparison:

a **b**

Multipole refinement (Ref. [S7]) **Computed**

Figure S1 Anisotropic thermal motion in **2** (90% probablity) from the results of a multipole refinement (as given as Fig. 2b in the main text) and from theory; both refer to T = 100 K.

Phonon localisation in 3

It is stated in the main text that the vibrations of the Os atoms in **3** are more distinctly localised at low frequencies than are those of the lighter Cr atoms in **1** and **2**. To illustrate this, we here calculated the projected phonon density of states, here denoted PDOS(ω), for all compounds and atom types under consideration. Then, we integrate this quantity over ω and normalise it:

$$\text{normalised IPDOS}(\omega) = \frac{\int_{-\infty}^{\omega} \text{PDOS}(\omega)\, d\omega}{\int_{-\infty}^{\infty} \text{PDOS}(\omega)\, d\omega}$$

This gives us the percentage of phonons for a given atom type that are found at a frequency at or lower than ω: the faster this term levels off at 100%, the more pronounced this is. We show the results in *Figure S2*. Indeed, the vibrational frequencies of Os in **3** are clearly more strongly localized below 500 cm^{-1} than the Cr frequencies in **1** and **2**.

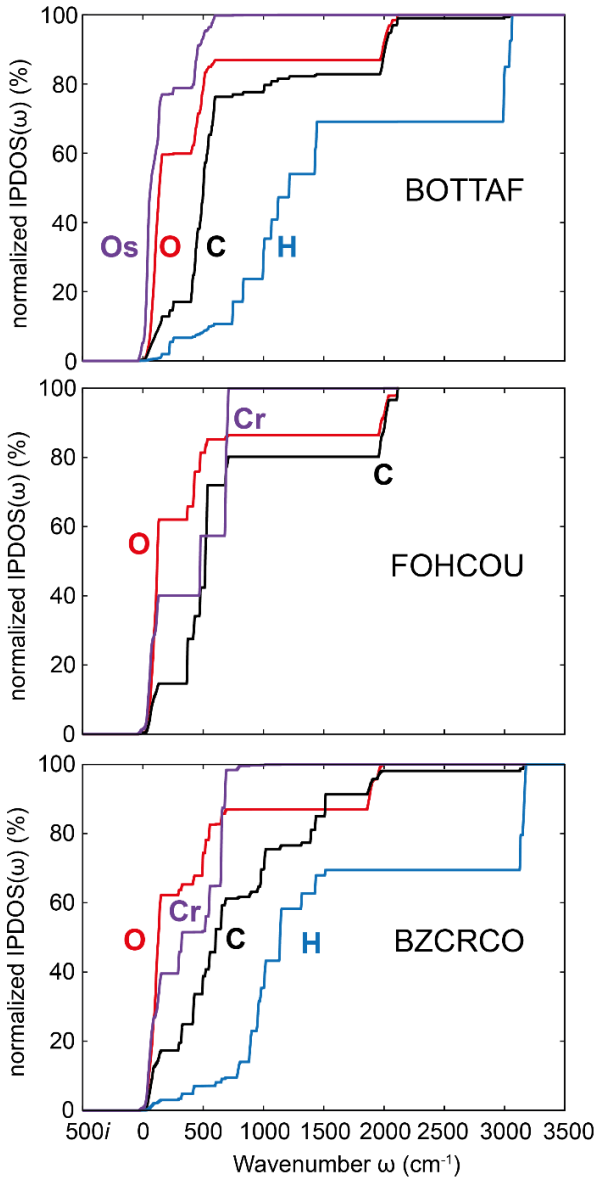

Figure S2 Comparison of the normalised IPDOS(ω) for all three investigated compounds. Around 80% of the Os-projected vibrations are found at wavenumbers below 423 cm^{-1}.

Anisotropic displacements at the LDA and M06L levels of theory

For comparison—and to rule out a fault of one particular DFT functional or level—we repeated the computations on **3** both with lower- and higher-rung functionals of DFT (*Table S4*).

At variance with the computations reported in the main text, the convergence criteria were slightly reduced to $\Delta E < 10^{-7}$ (10^{-5}) eV/cell for electronic (structural) optimisation, respectively, which still corresponds to tight settings but was required to make the M06L computations feasible. The tolerance to find the experimental space group within PHONOPY [S5] was set to 10^{-4} Å for the LDA and M06L calculations.

Table S4 Principal elements of computed anisotropic displacement tensors for both osmium atoms in **3**, obtained at different levels of theory and compared to experiments. No systematic improvement is seen with the higher-rung functional: overall, for Os(1), the PBE+D3(BJ) approach also used in the main text shows the best performance among the three methods, whereas for Os(2) M06L performs best among the three methods tested here.

	Os(1)			**Os(2)**		
	U_1	U_2	U_3	U_1	U_2	U_3
	(all in 10^{-4} Å^2)			(all in 10^{-4} Å^2)		
Expt.	**37**	**41**	**62**	**32**	**51**	**67**
LDA	20	22	31	26	28	29
M06L	18	21	34	21	31	45
PBE+D3(BJ)	24	26	37	24	29	32

Optimised structures

In *Table S5*, we summarise the lattice parameters for the optimised structural models of all three compounds under study. Full data regarding structures and ADPs are provided in CIF format (`DFT_1.cif`, `DFT_2.cif`, and `DFT_3.cif`).

Table S5 Optimised lattice parameters from DFT-D relaxation.

compound	**1**	**2**	**3**
a (Å)	11.5694	6.0197	7.3647
b (Å)	10.9308	10.8418	13.4814
c (Å)	6.2129	6.5446	13.6756
β (°)	90	101.21	102.01

Supplementary references

[S1] Bruker (2009). SAINT+, Version 6.02. Bruker AXS Inc., Madison, Wisconsin, USA.

[S2] G. M. Sheldrick, *Acta Crystallogr., Sect. C*, 2015, **71**, 3–8.

[S3] J. George, A. Wang, V. L. Deringer, R. Wang, R. Dronskowski and U. Englert, *CrystEngComm*, 2015, **17**, 7414–7422.

[S4] Nonetheless, we remark that for future studies targeting room-temperature measurements, there exist computational approaches for predicting the lattice expansion from first principles as well. See, for example: S. Q. Wang, *Appl. Phys. Lett.*, 2006, **88**, 061902.

[S5] (a) A. Togo, F. Oba and I. Tanaka, *Phys. Rev. B*, 2008, **78**, 134106; (b) A. Togo and I. Tanaka, *Scr. Mater.*, 2015, **108**, 1–5.

[S6] N. J. Lane, S. C. Vogel, G. Hug, A. Togo, L. Chaput, L. Hultman and M. W. Barsoum, *Phys. Rev. B*, 2012, **86**, 214301.

[S7] L. J. Farrugia, C. Evans, D. Lentz and M. Roemer, *J. Am. Chem. Soc.*, 2009, **131**, 1251–1268.